European Journal of Nuclear Medicine and Molecular Imaging (2019) 46:1019–1036
https://doi.org/10.1007/s00259-018-4181-2

REVIEW ARTICLE

Osteoid osteoma: multimodality imaging with focus on hybrid imaging

Ujwal Bhure[1] · Justus E. Roos[1] · Klaus Strobel[1]

Received: 1 June 2018 / Accepted: 25 September 2018 / Published online: 19 October 2018

Abstract

Osteoid osteoma is a painful, benign, osteoblastic lesion that occurs in younger patients and affects the extremities or the axial skeleton. While plain film findings may suggest the diagnosis, in complex anatomical regions such as the spine, pelvis, wrist and foot advanced imaging modalities are often required. A typical nidus surrounded by sclerosis or cortical thickening characterizes osteoid osteoma on plain radiography and CT. MR is the cross-sectional imaging modality of choice for most musculoskeletal disorders. Unfortunately, extensive accompanying bone marrow oedema, soft-tissue alterations, difficulty detecting the nidus, and lesion locations close to a joint (with reactive arthritis) may make a confident diagnosis of osteoid osteoma by MR imaging difficult. Hybrid imaging with bone-seeking tracers such as SPECT/CT with ^{99m}Tc-labelled bisphosphonates or PET/CT with ^{18}F-labelled sodium fluoride (^{18}F-NaF) combines high radionuclide uptake with morphological details and provides accurate diagnosis of osteoid osteoma and additional information for treatment planning. FDG is not the recommended PET tracer because osteoid osteoma is normally FDG-negative, although some osteoid osteomas may show increased FDG uptake. Osteoblastoma, Brodie's abscess and stress fractures may mimic osteoid osteoma on imaging and clinical presentation. Once identified as the pain generator, destruction of the osteoid osteoma nidus by ablation or resection techniques usually leads to complete healing. Image-guided drill excision and radiofrequency ablation are widely used interventions. We review the presentation of osteoid osteoma across all imaging modalities, with special focus on hybrid imaging techniques.

Keywords Osteoid osteoma · Hybrid imaging · SPECT/CT · MR · PET/CT · Bone scintigraphy

Introduction

Osteoid osteoma is a benign but painful skeletal osteoblastic lesion that generally affects younger, predominantly male patients with a peak incidence in the second decade of life. The lesions are generally smaller than 2 cm, and when detected are very amenable to treatment. Bergstrand was the first to describe osteoid osteoma in 1935, and Jaffe subsequently characterized osteoid osteoma as a distinct clinical entity [1, 2]. Osteoid osteoma is a benign bone-forming lesion morphologically composed of a central nidus of vascular osteoid tissue surrounded by extensive formation of compact bone. The osteoid within the nidus may undergo various degrees of calcification and is associated with irregular trabecular bone formation. Periosteal reaction with formation of compact lamellar bone can be seen, as well as perilesional dense sclerosis within the host bone due to pressure exerted by the highly vascularized lesion [3–6].

Osteoid osteoma is the third most common benign bone tumour after enchondroma and nonossifying fibroma [7–9]. The pathogenesis of osteoid osteoma remains unclear; some authors suggest that it is a true benign osteoblastic neoplasm, while others believe it may represent unusual healing or an inflammatory process [10–12]. The classic clinical presentation includes local pain, often worse at night and relieved by nonsteroidal

✉ Klaus Strobel
klaus.strobel@luks.ch

[1] Department of Radiology and Nuclear Medicine, Cantonal Hospital Lucerne, Lucerne, Switzerland

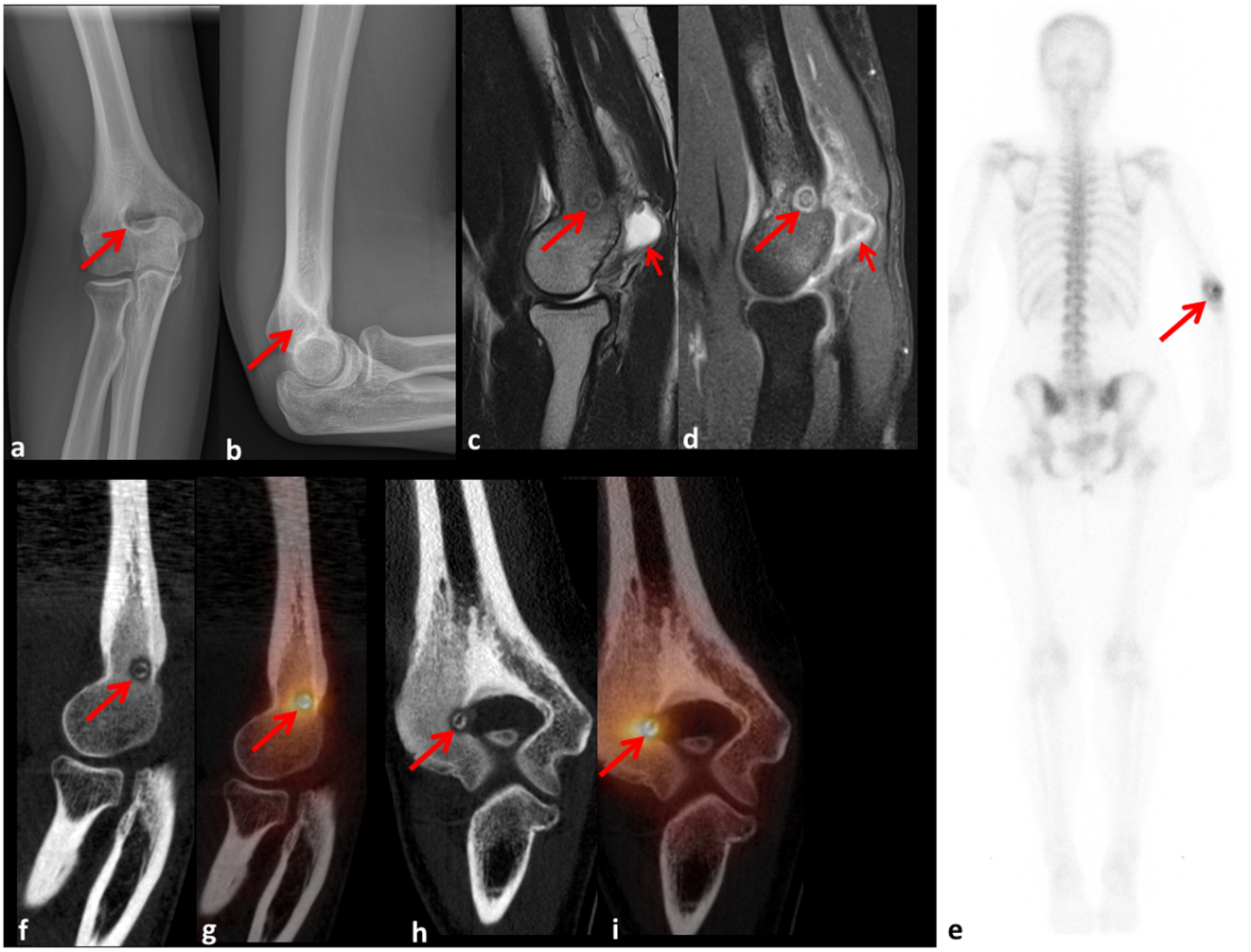

Fig. 1 Osteoid osteoma in a 19-year-old woman with effusion and pain in the left elbow. **a**, **b** The small nidus (*arrows*) adjacent to the olecranon fossa is difficult to see on radiographs. **c**, **d** Sagittal T2-weighted (**c**) and contrast-enhanced T1-weighted (**d**) MR images show the nidus (*arrows*) in the distal humerus and arthritis with effusion (*small arrows*). **e** The whole-body planar bone scan image shows the "double density" sign (*arrow*). **f**–**i** Sagittal (**f**) and coronal (**h**) CT images show the nidus (*arrow*) near the olecranon fossa and sagittal (**g**) and coronal (**i**) SPECT/CT images show increased uptake (*arrows*)

antiinflammatory drugs (NSAIDs) [13]. However, the location of the pain is sometimes misleading since it can be referred to a nearby joint, creating clinical ambiguity that can hamper the imaging workup. Localized swelling may be attributed to the highly vascular nature of this benign tumour, which can be well depicted and evaluated by scintigraphy and MRI [14–18]. Local production of prostaglandins, to levels 100 to 1,000 times higher than in normal bone, plays an important role in the classic clinical presentation of pain during day and night, which typically responds very well to NSAIDs [19, 20]. Other clinical features associated with osteoid osteoma depend on the specific location of the lesion, and include swelling, limp, painful scoliosis, growth disturbance, joint stiffness and contracture [8].

Patients with osteoid osteoma located close to joints may present with joint pain, swelling and joint effusions that may mimic arthritis [21] (Fig. 1). Atypical clinical presentations without the painful triad are possible, especially with osteoid osteomas located in the phalanges, where soft-tissue swelling is often the primary clinical feature [22, 23]. Osteoid osteomas may occur anywhere within the axial or appendicular skeleton, with the majority (>50%) occurring in lower extremity locations such as the femur (Fig. 2) or tibia [9, 24]. Two thirds of the femoral lesions are situated in the intertrochanteric or intracapsular regions of the hip. The humerus is another common location for osteoid osteoma. Within the bone, osteoid osteomas preferentially involve the cortex of long bones, usually in the diaphysis (Fig. 3) or metadiaphysis [9, 25]. Approximately 10% to 20% of

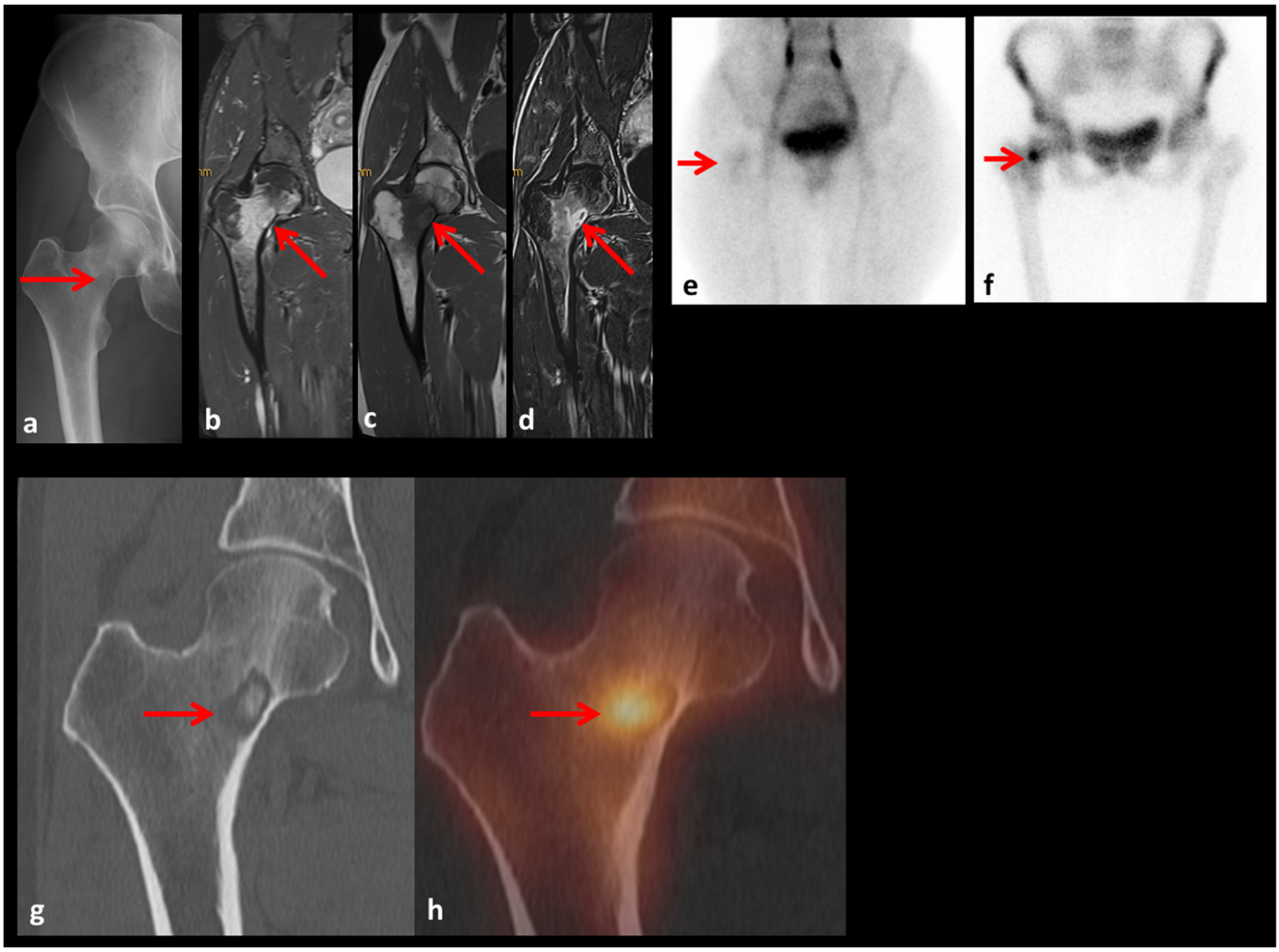

Fig. 2 Osteoid osteoma of the right femoral neck in a 48-year-old woman. **a** The radiograph shows osteolysis in the medial femoral neck with a central nidus (*arrow*). **b**–**d** The coronal STIR MR image (**b**) shows extensive bone marrow oedema (*arrow*), the T1-weighted image (**c**) shows a hypointense subcortical lesion (*arrow*) and demarcation of the hypointense nidus (*arrow*), and the contrast-enhanced T1-weighted image (**d**) shows increased surrounding contrast enhancement. **e**, **f** The early phase planar bone scan image of the pelvis (**e**) shows slightly increased uptake in the femoral neck (*arrow*) and the late phase bone scan image (**f**) shows markedly increased focal uptake (*arrow*) in the femoral neck with surrounding mildly increased uptake ("double density" sign). **g**, **h** The CT image (**g**) and the fused SPECT/CT image (**h**) show the central nidus with increased uptake (*arrow*)

osteoid osteomas occur in the spine (Fig. 4), most commonly in the lumbar spine with a predilection for the posterior elements. The vertebral body is often spared, being involved in only 10% of spinal lesions [26, 27]. Uncommon locations for osteoid osteoma include the skull (Fig. 5), hand, ankle and foot (Figs. 6 and 7).

Classification

Kayser et al. classified osteoid osteomas based on their location within the bone as follows: subperiosteal, intracortical, endosteal and medullary [6]. Intracortical lesions are most common, representing approximately 75% of lesions (Fig. 8). Medullary osteoid osteomas account for around 20%, and subperiosteal and endosteal lesions account for the remaining 5% (Fig. 9). Intracortical osteoid osteomas, known as the "classic" type, are usually seen in the diaphysis or metaphysis of the long tubular bones, such as the tibia and femur, where a radiolucent nidus is located in the centre of fusiform cortical thickening.

Subperiosteal osteoid osteomas are located on the external aspect of the cortex, and are usually seen along the medial aspect of the femoral neck, hands, feet and neck of the talus. Medullary osteoid osteomas are typically juxta-articular in location, and are often seen in the femoral neck, hands, feet and posterior elements of the spine. Endosteal osteoid osteomas are located on the internal aspect of the

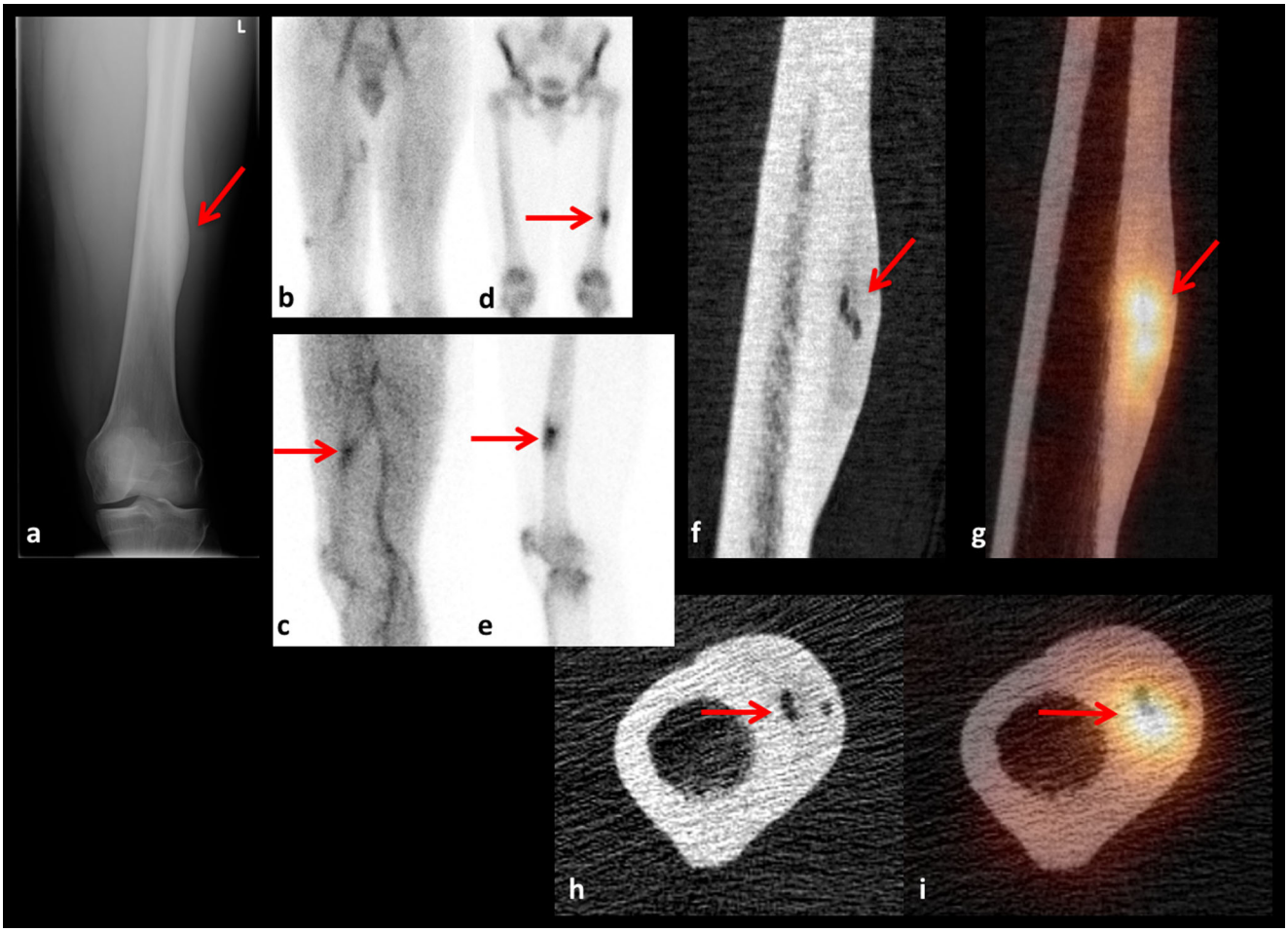

Fig. 3 Osteoid osteoma of the left femur in a 42-year-old man. **a** The radiograph shows a small subperiosteal nidus (*arrow*) and thickening of the lateral cortex. **b**, **c** The early phase planar bone scan images show slightly increased uptake (*arrow*) in the anterolateral aspect of the left femur. **d**, **e** The late phase bone scan images show markedly increased uptake (*arrows*) in the anterolateral left femur. **f**, **h** The coronal (**f**) and axial (**h**) CT images show a subperiosteal nidus (*arrows*) and cortical thickening. **g**, **I** The coronal (**g**) and axial (**I**) SPECT/CT images show Increased uptake (*arrows*)

cortex and may cause atypical circumferential cortical thickening [9, 11]. Kayser et al. suggested that inward migration of an osteoid osteoma caused by continuing remodelling of the bone due to subperiosteal deposition and endosteal erosion can result in a shift of the nidus from a subperiosteal to an intracortical or endosteal location, or even to an intramedullary location [6].

Plain radiography

The radiographic appearance of osteoid osteoma depends on its location within the involved bone. The most common "targetoid" appearance is a cortical-based lucency measuring less than 2 cm, with central calcification seen within a radiolucent nidus, especially in larger lesions. This radiolucent nidus is surrounded by fusiform osteosclerosis involving one side of a long bone diaphysis. This reactive sclerosis and cortical thickening may occasionally obscure the nidus [28]. The degree of sclerosis surrounding the nidus is less in epiphyseal and metaphyseal lesions than in diaphyseal lesions; medullary lesions also exhibit less sclerosis than their intracortical counterparts. Subperiosteal lesions produce minimal sclerosis and may appear as soft-tissue lesions adjacent to the affected bone, which reveals irregular bony resorption [25]. Plain radiography might fail to depict an osteoid osteoma in complex anatomical areas such as the spine, pelvis, skull or foot, where superimposed bony structures can obscure the lesion [29, 30]. Jordan et al., in a meta-analysis of 223 patients with proven osteoid osteoma, found a detection rate of only 66% by plain radiography [31].

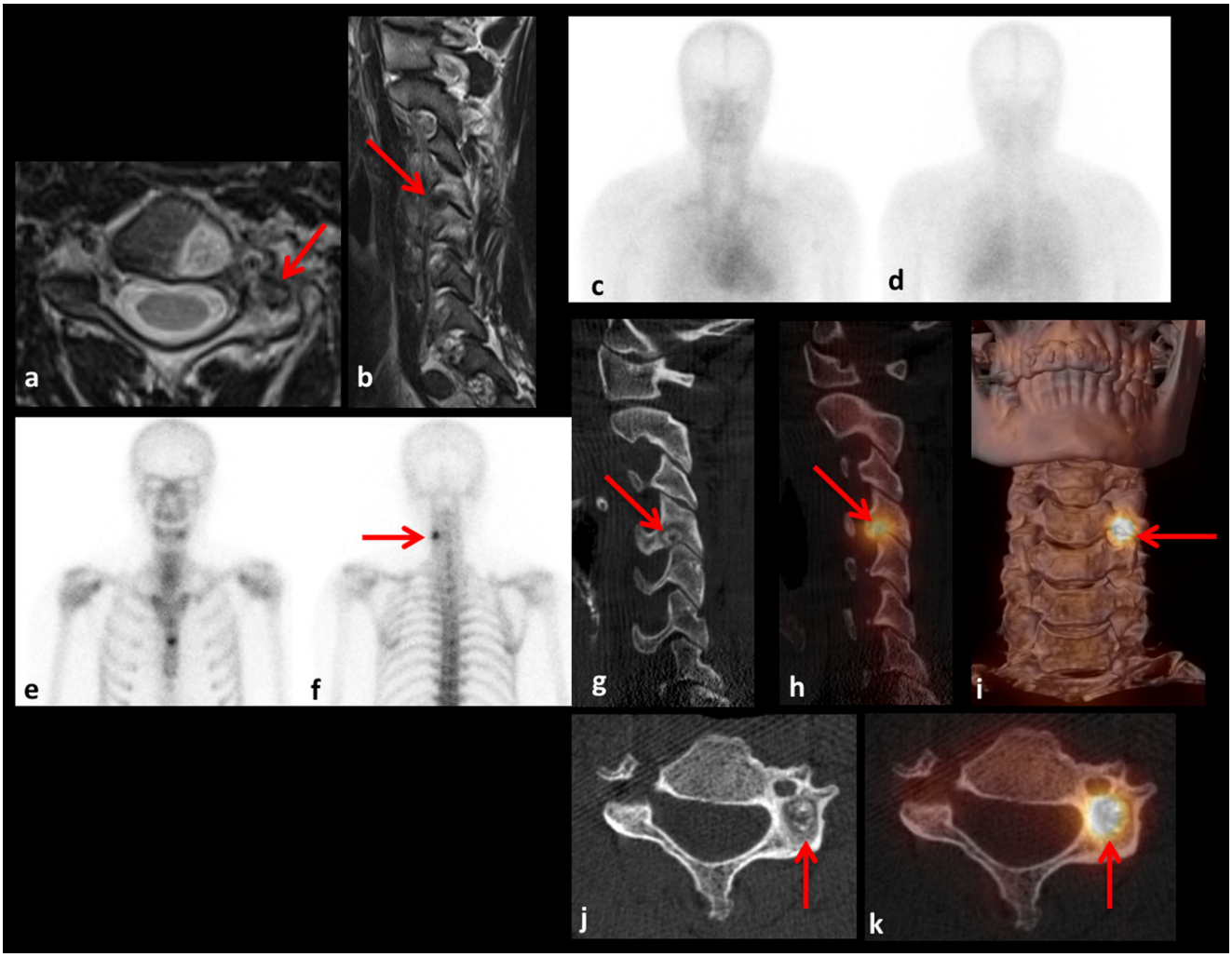

Fig. 4 Osteoid osteoma in a 23-year-old man with pain in the neck for several months. **a**, **b** The axial (**a**) and sagittal (**b**) T2-weighted MR images show a hypointense nidus (*arrows*) in the C4 arch with extensive bone marrow oedema in the adjacent vertebral bodies and posterior elements. **c**, **d** The anterior (**c**) and posterior (**d**) early phase planar bone scan images show no increased uptake. **e**, **f** The anterior (**e**) and posterior (**f**) late phase planar bone scan images show increased focal uptake (*arrow*) in the left mid-lateral aspect of the cervical spine. **g**, **j** The sagittal (**g**) and axial (**j**) CT images show a small nidus (*arrows*) in the C4 arch adjacent to the facet joint. **h**, **I**, **k** The sagittal (**h**), axial (**k**) and 3D (**I**) SPECT/CT images show increased uptake (*arrows*) in the osteoid osteoma

Computed tomography

CT is far superior to plain radiography for the detection and characterization of osteoid osteoma [9, 24, 28, 32]. Thin-section CT reconstructed with bone window and level settings, and reviewed with multiplanar reformats is the optimum method for the visualization of osteoid osteoma. The typical lesion is seen as a well-defined round or oval focal area of soft-tissue attenuation, less dense than, and surrounded by, variable amounts of osteosclerosis. Mineralization or calcification of the nidus can be characterized by CT as punctate, amorphous or ring-like. Osteoid osteomas are frequently surrounded by thin curvilinear or serpentine low-density grooves in the surrounding bone, the so-called “vascular groove” sign. Liu et al. found that the vascular groove sign has moderate sensitivity but high specificity in the discrimination of osteoid osteomas from other radiolucent bone lesions (Fig. 10a) [33]. CT is superior to plain radiography for detecting osteoid sarcoma, especially in cases where the nidus is obscured by surrounding sclerosis on radiography [24, 34, 35]. CT is especially useful for the detection of spinal osteoid osteomas, which are seen as low-density lesions in the posterior elements of the vertebral column associated with reactive sclerosis of the ipsilateral pedicle, lamina or transverse process. Several authors have

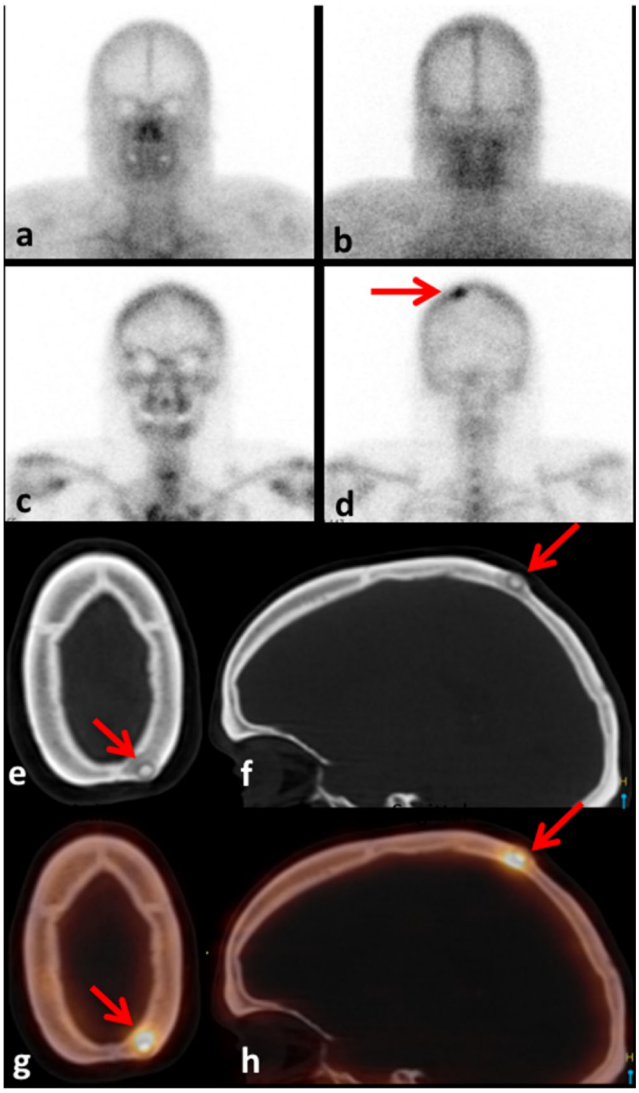

Fig. 5 Osteoid osteoma in the skull of a 44-year-old man. **a**, **b** The early phase planar bone scan images show no increased uptake. **c**, **d** The anterior (**c**) and posterior (**d**) late phase planar bone scan images show increased focal uptake (*arrow*) in the parietal paramedian skull. **e**, **f** The axial (**e**) and sagittal (**f**) CT images show the nidus (*arrows*) in the diploë. **g**, **h** The axial (**g**) and sagittal (**h**) SPECT/CT images show increased uptake (*arrows*). A slight mismatch between the nidus and uptake caused by patient movement is apparent

reported a 100% detection rate of osteoid osteoma in the spine [29, 30] and Jordan et al. found a 96% detection rate of osteoid osteoma in the foot using CT [31].

Magnetic resonance imaging

Although many studies have shown that CT is superior to MRI for detecting and characterizing osteoid osteoma [36–38], MRI occasionally adds incremental value to the characterization of these lesions. A 35% risk of misdiagnosis with MRI as the primary imaging modality has been reported [31, 36, 37], since in small lesions the nidus and the surrounding cortex may show similar MRI signal intensity. Gadolinium enhancement might improve the detection of osteoid sarcoma by dynamic MRI since it increases osteoid osteoma conspicuity [39]. The MRI appearance of osteoid osteoma is variable, commonly exhibiting low to intermediate T1-weighted signal and heterogeneous high signal with T2-weighted and STIR sequences [24, 36, 37]. Central nidus calcifications show low signal with both T1-weighted and T2-weighted sequences [7]. Most osteoid osteomas enhance diffusely after gadolinium administration as a result of their intrinsic vascularity. Rim enhancement may be heterogeneous. Perilesional sclerosis is seen as fusiform low signal with both T1-weighted and T2-weighted sequences. MRI typically shows intense surrounding bone marrow and soft-tissue oedema.

Bone scintigraphy and SPECT/CT

Bone scintigraphy with ^{99m}Tc-labelled bisphosphonates has been used for decades for the diagnosis of osteoid osteoma, with a reported sensitivity of nearly 100% [40, 41]. The classic bone scintigraphic finding is the "double density" sign, where a central focus of very high activity corresponding to the nidus of the osteoid osteoma is surrounded by a larger area of less intense radiopharmaceutical uptake, representing the host bone tumour response [42]. This sign is very specific for osteoid osteoma in the appendicular skeleton; however, it is less frequently seen in spinal lesions because of less reactive osteosclerosis in the vertebrae [42, 43]. The presence of the pathognomonic double density sign allows differentiation of osteoid osteoma from Brodie's abscess, stress reaction and metastasis [7, 9]. In comparison with planar imaging, single photon emission computed tomography (SPECT) imaging with three-dimensional reconstruction techniques has better spatial resolution and is therefore able to detect smaller lesions [44, 45]. To further improve the detection and characterization of osteoid osteoma, SPECT examinations are typically followed by a coregistered or stand-alone CT examination. The fused functional and structural information provided by most current SPECT/CT scanners has led to this modality becoming the one-stop imaging tool that is able to diagnose osteoid osteoma with the highest accuracy [46–50]. Sharma et al. retrospectively investigated 31 patients and found significantly higher

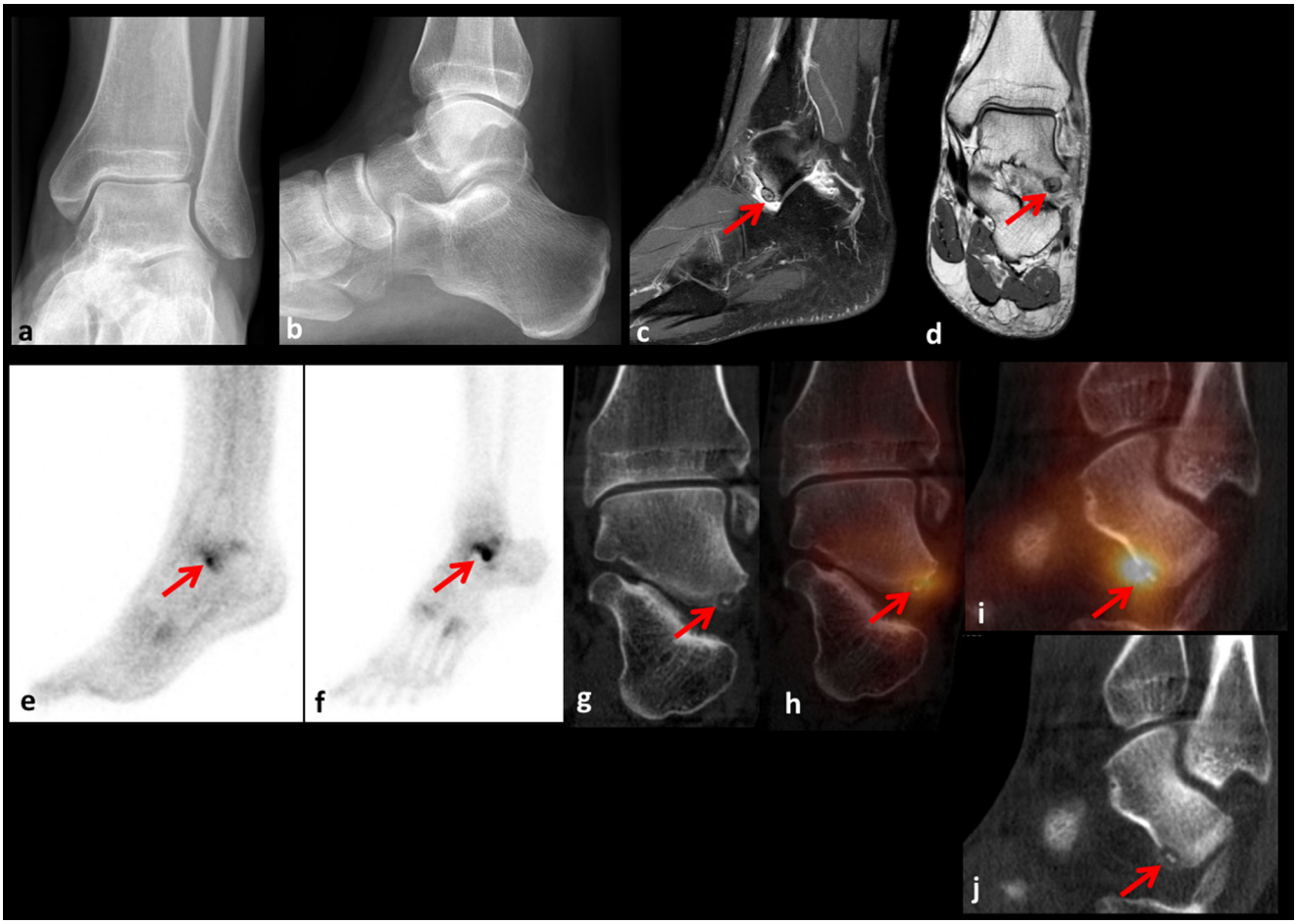

Fig. 6 Osteoid osteoma on the lateral border of the talus in a 29-year-old man with pain for 2 years. **a**, **b** The radiographs show no abnormality. **c**, **d** The sagittal STIR MR image (**c**) and coronal T1-weighted image (**d**) show the nidus (*arrows*) and surrounding bone marrow oedema. **e**, **f** The planar bone scan images (**e** early phase, **f** late phase) show increased focal uptake (*arrows*) at the border of the talus. **g**, **j** The coronal (**g**) and sagittal (**j**) CT images show the nidus (*arrows*). **h**, **I** The coronal (**h**) and sagittal (**I**) SPECT/CT images show corresponding increased uptake (*arrows*)

sensitivity, specificity and accuracy with SPECT/CT (all 100%) than with CT (77.8%, 92.3% and 83.8%, respectively) or planar bone scintigraphy (100%, 38.4% and 74.1%, respectively) [49].

^{18}F-NaF PET/CT

^{18}F-Labelled sodium fluoride (^{18}F-NaF) is a bone-seeking radiotracer with uptake characteristics comparable to those of conventional ^{99m}Tc-labelled bisphosphonates used for "classic" bone scintigraphy [51, 52]. Due to a higher lesion to background ratio, better spatial resolution, and combination with diagnostic CT, ^{18}F-NaF PET/CT shows higher accuracy in the diagnosis of bone metastases than planar bone scintigraphy, SPECT and SPECT/CT [53, 54]. ^{18}F-NaF PET/CT has also been used to evaluate benign skeletal diseases such as spondyloarthropathies/sacroiliitis [55], foot pain [56], trauma [57], osteonecrosis [58] and insufficiency fracture [59], and in the assessment of bone grafts [60]. Reimbursement issues, cost and limited availability have prevented the widespread use of this tracer in many countries. ^{18}F-NaF PET/CT is excellent for imaging osteoid osteomas because very high uptake in the nidus can be expected, sometimes accompanied by markedly increased uptake in the surrounding bone (Fig. 10b). Together with the exact location of the osteoid osteoma in relation to joints and the surrounding soft-tissue structures, ^{18}F-NaF PET/CT provides all relevant diagnostic information and supports interventional or surgical treatment planning. Several case reports have demonstrated the potential of ^{18}F-NaF PET/CT to detect osteoid osteomas in children and adults, for example, in the acetabulum [61], sacrum [62] (Fig. 11a, b) and femur [63].

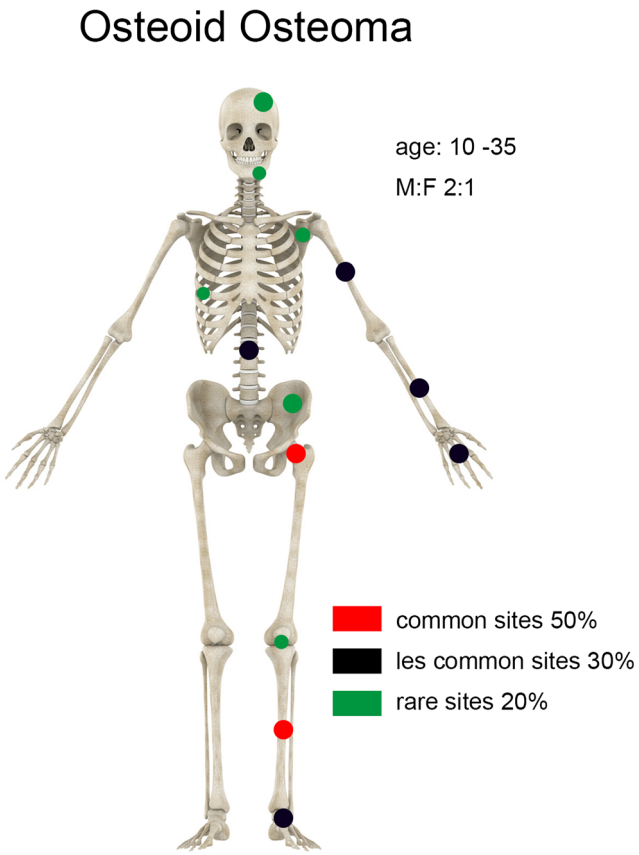

Fig. 7 Common and less common sites of osteoid osteoma in the skeleton

^{18}F-FDG PET/CT

^{18}F-FDG is the most frequently used PET tracer worldwide. Since FDG accumulates in proliferating cancer cells, the vast majority of FDG PET/CT applications are related to the imaging of malignant tumours. Although bone-seeking tracers are recommended for imaging osteoid osteoma, FDG may intensely accumulate in osteoid osteoma as shown in several case reports. Lim et al. reported the case of a patient showing intense FDG uptake in an osteoid osteoma in the distal metaphysis of the tibia [64]. Imperiale et al. reported the cases of three patients with osteoid osteoma in the femur, spine (Fig. 12), and talus with high focal FDG uptake [65]. The authors also utilized FDG PET/CT to monitor response to therapy. They found significant decreases in FDG uptake after successful radiofrequency ablation (RFA). In contrast to these results, FDG PET/CT may also produce false-negative results in the detection of osteoid osteoma. Aoki et al. compared FDG uptake in benign and malignant bone tumours and found that the osteoid osteoma in two patients did not show significant FDG uptake (standardized uptake value <2.0) [66] (Fig. 13). It currently remains unclear which cells are responsible for FDG uptake in osteoid osteoma since autoradiography studies have not yet been performed. Since osteoblasts and activated inflammatory cells are present in osteoid osteoma, both could be the reason for positive FDG imaging. FDG uptake may correlate with pain or "activity" of osteoid osteomas, and therefore could direct treatment so that optimal treatment is more likely to be achieved in FDG-positive than in FDG-negative osteoid osteoma lesions. However, further evaluation of this possible relationship is needed.

Osteoid osteoma mimickers

Some skeletal lesions can mimic the radiological and clinical appearance of osteoid osteoma, the most common being Brodie's abscess. However, unlike osteoid osteoma, in Brodie's abscess the sequestrum is often irregular in shape and the inner margin of the area of lucency is not smooth [7, 67]. Other bone lesions mimicking osteoid osteoma include chondroblastoma, osteoblastoma, stress fracture, osteofibrous dysplasia and adamantinoma. Chondroblastomas are epiphyseal and intramedullary in location, whereas osteoid osteomas are generally diaphyseal and intracortical [7, 68]. Osteoblastomas are frequently located in the axial skeleton (particularly the spine and mandible), are generally larger than osteoid osteomas, can be locally aggressive and expansile, and have less-reactive perilesional sclerosis than osteoid osteomas [7]. Additionally, pain in osteoblastoma is usually not worse at night and is less likely to be relieved by NSAIDs [69]. Stress fractures in the lower extremities produce focal cortical thickening similar to osteoid osteoma and can be difficult to distinguish on plain radiography. Cross-sectional imaging techniques such as CT are helpful for separating osteoid osteoma from stress fracture, since the latter presents with a discrete fracture instead of a central nidus. Features of osteoid osteoma and the differential diagnoses of osteoid osteoma by various imaging modalities are summarized in Tables 1 and 2.

Management

Some osteoid osteomas show a self-limited course with spontaneous resolution of symptoms [70]. Medical or

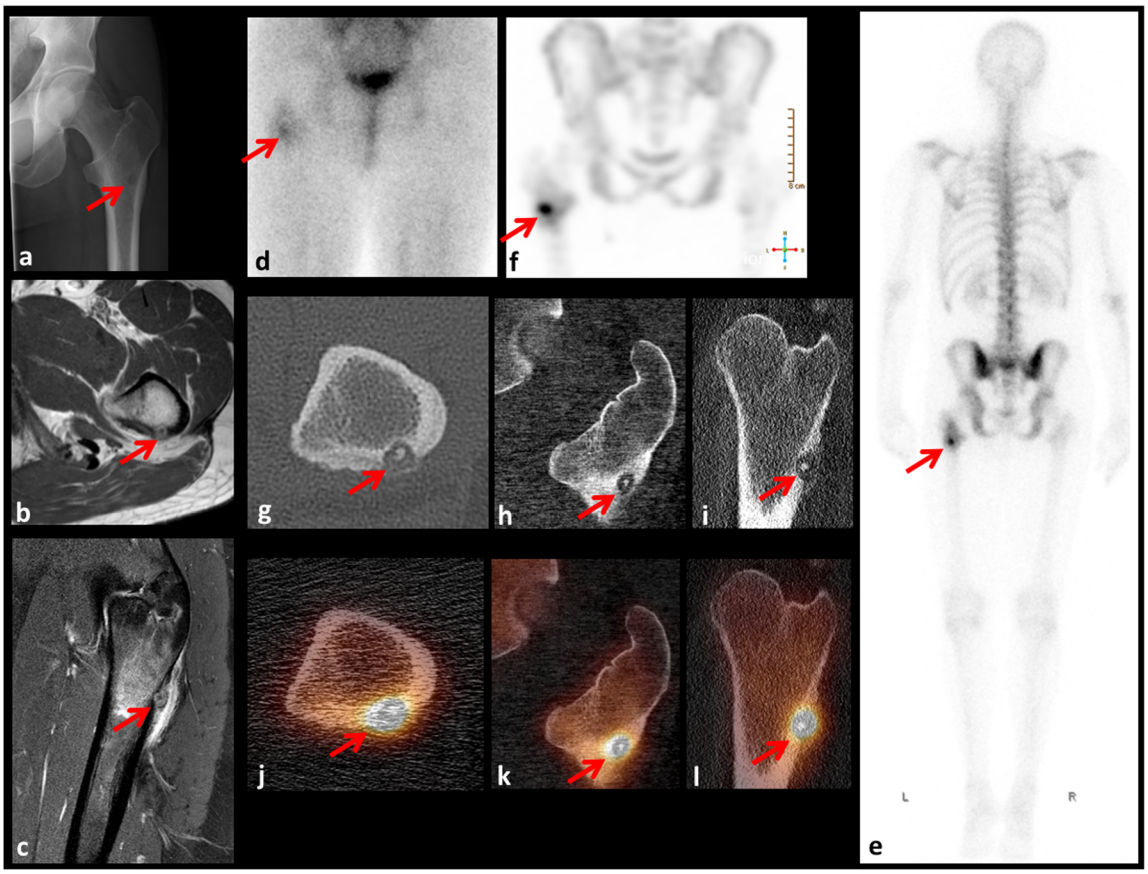

Fig. 8 Osteoid osteoma of the left proximal femur in a 42-year-old man. **a** The radiograph shows a small cortical nidus (*arrow*). **b**, **c** The T1-weighted axial (**b**) MR image shows an intracortical nidus (*arrow*) and the coronal fat-saturated T1-weighted image (**c**) shows the nidus (*arrow*) with contrast enhancement of the surrounding bone marrow and adjacent soft tissue. **d**–**f** The posterior planar bone scan images (**d** early phase, **e** late phase) and the MIP image (**f**) of the pelvis show increased focal uptake (*arrows*) in the proximal left femur. **g**–**I** The axial (**g**), coronal (**h**) and sagittal (**i**) CT images show an intracortical nidus (*arrows*) with adjacent periosteal reaction. **j**–**l** The axial (**j**), coronal (**k**) and sagittal (**l**) SPECT/CT images show corresponding increased uptake (*arrows*)

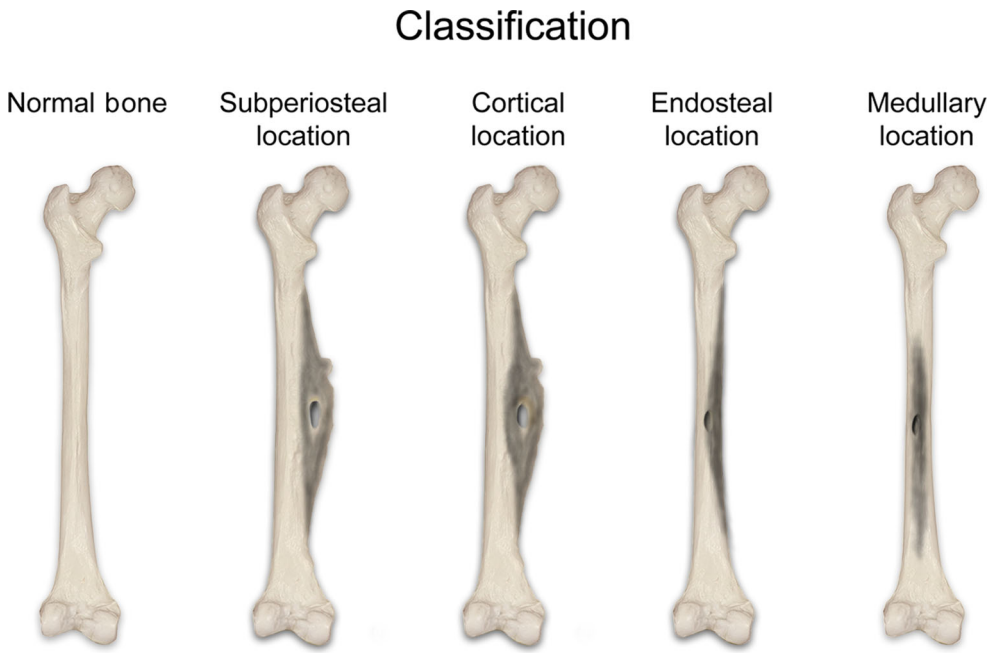

Fig. 9 Classification scheme with regard to the location of osteoid osteomas within the long bones

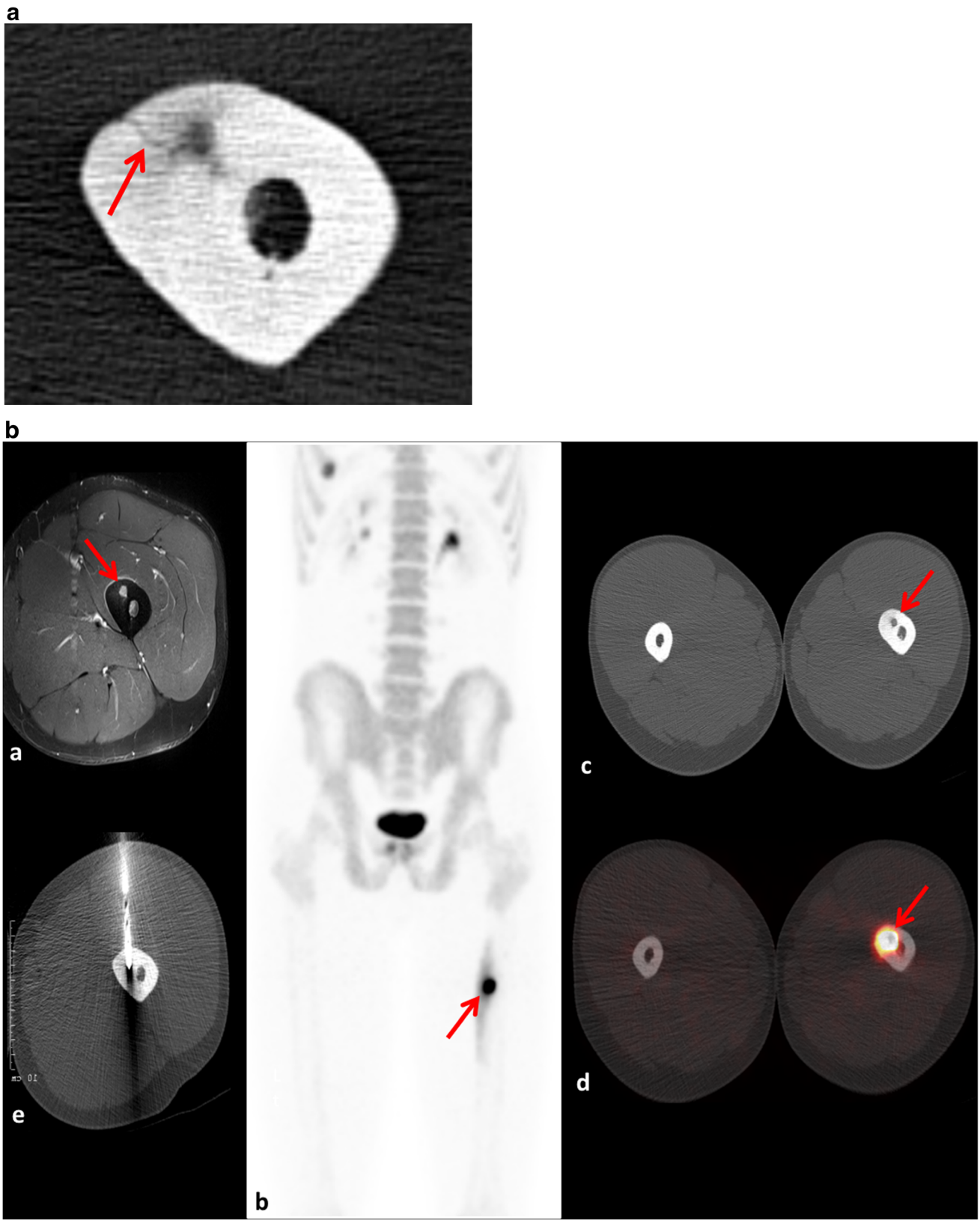

Fig. 10 **a** Axial CT in the same patient from **b** shows a thin curvilinear or serpentine low-density groove leading to the nidus, the so called "vascular groove" sign. **b** Osteoid osteoma of the left proximal femur in an 18-year-old man. **a** The axial contrast-enhanced T1-weighted MR image shows an enhancing nidus (*arrow*) in the cortex of the proximal femoral diaphysis. **b** The ^{18}F-NaF PET/CT MIP image shows markedly increased focal uptake (*arrow*) with slightly increased uptake in the thickened surrounding cortex. **c**, **d** The axial CT image (**c**) and fused PET/CT image (**d**) show the cortical nidus (*arrows*). **e** CT-guided drill excision was performed for therapy

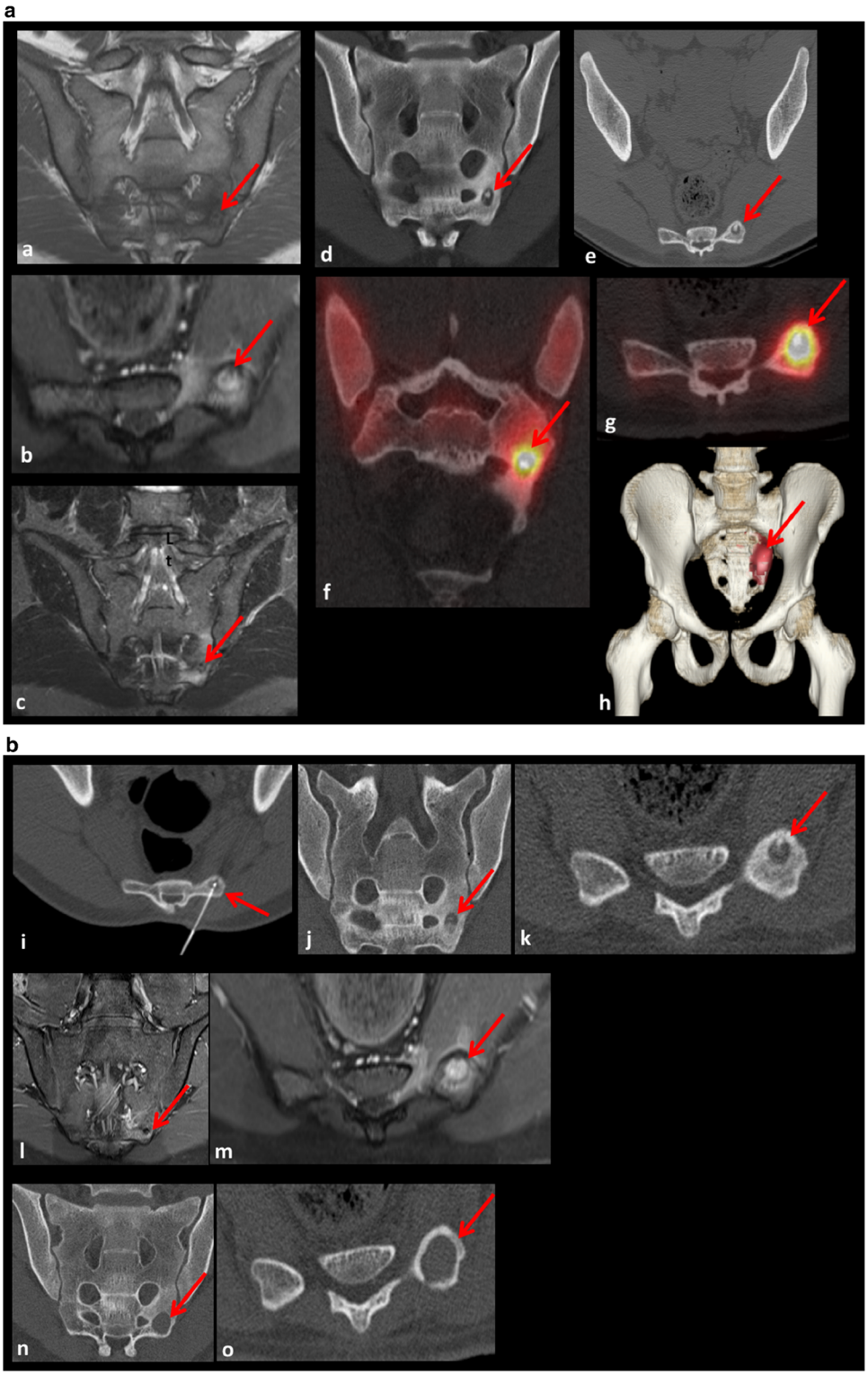

Fig. 11 Osteoid osteoma of the left sacrum in an 18-year-old man. **a** The oblique coronal T1-weighted MR image shows a hardly detectable nidus (*arrow*). **c** The T2-weighted oblique coronal image shows the nidus (*arrow*) and surrounding bone marrow oedema. **b** The axial contrast-enhanced T1-weighted image shows enhancement of the nidus (*arrow*) and the surrounding bone marrow. **d**, **e** The oblique coronal (**d**) and axial (**e**) CT images show the easily detectable nidus (*arrows*). **f**–**h** The fused coronal (**f**) and axial (**g**) ^{18}F-NaF PET/CT images and 3D MIP image (**h**) show intense focal uptake (*arrows*) in the osteoid osteoma. **i** CT-guided radiofrequency ablation was performed; note the probe (*arrow*) in the nidus. **j**–**m** The coronal (**j**) and axial (**k**) CT images and MR images (**l**, **m**) show a small residual or recurrent nidus (*arrows*) with oedema and contrast enhancement. **n**, **o** Because of persistent pain 4 months after radiofrequency ablation, open resection was performed and the coronal (**n**) and axial (**o**) CT images show the resection defect (*arrows*) and complete removal of the nidus

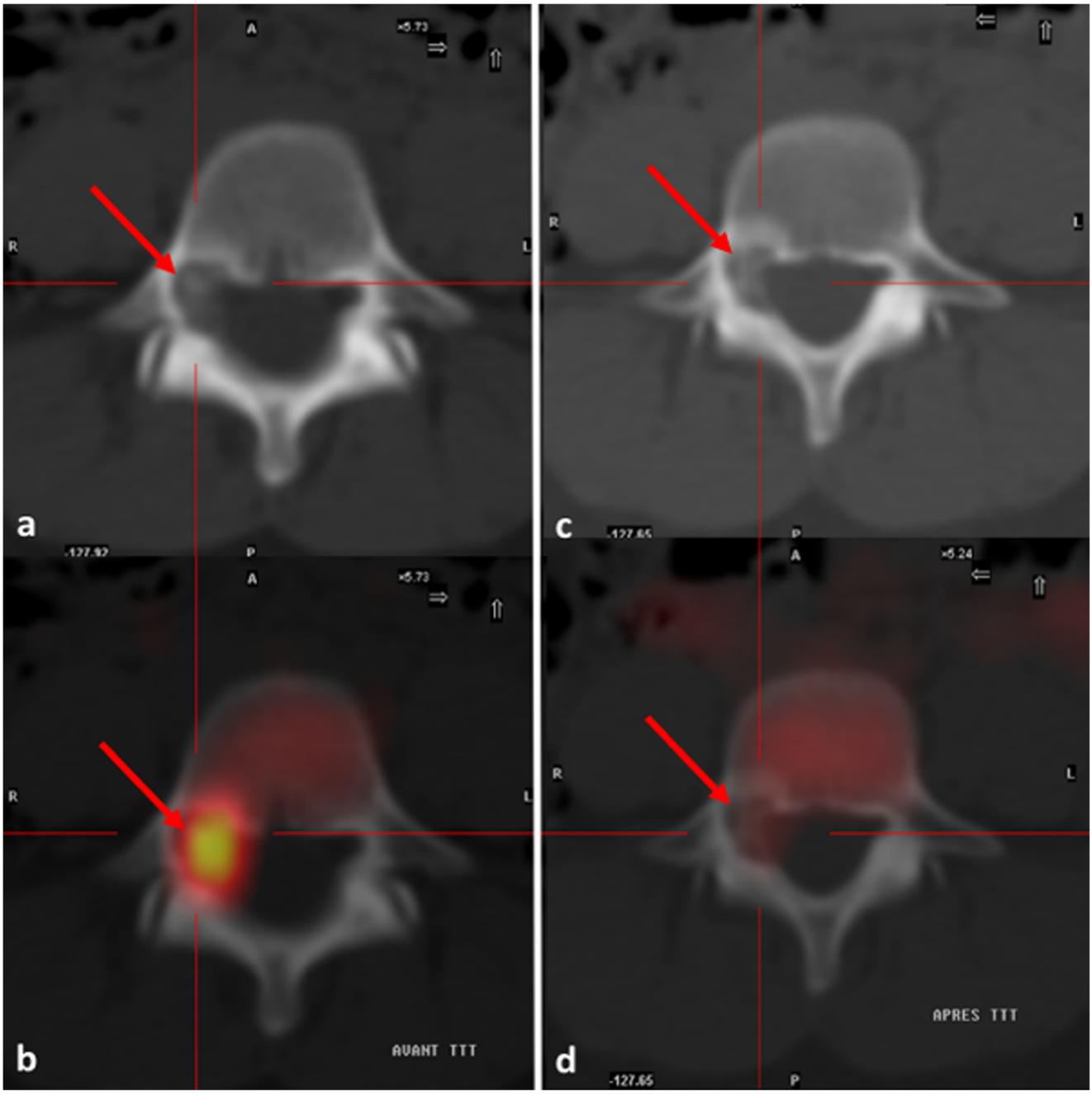

Fig. 12 Osteoid osteoma in a 28-year-old woman with pain in the lumbar spine. **a**, **b** The CT image (**a**) shows osteoid osteoma (*arrow*) in the right L5 pedicle and the fused PET/CT image (**b**) shows increased FDG uptake (*arrow*). **c**, **d** After radiofrequency ablation, the CT image (**c**) shows destruction of the nidus (*arrow*) and the fused PET/CT image (**d**) shows absence of FDG uptake (*arrow*). Image courtesy of Dr. Alessio Imperiale, Nuclear Medicine, University Hospital Strasbourg, France

conservative management with NSAIDs can be the initial treatment [10, 71]. However, long-term NSAID therapy may not be tolerated by patients because of undesirable side effects. If conservative treatment fails, surgical or minimally invasive percutaneous treatments, with the aim of destroying the nidus completely, are indicated. Surgical treatment with open en-bloc resection or curettage has high success rates but is invasive and has potential disadvantages including the risks of general anaesthesia, difficulty in locating the lesion intraoperatively,

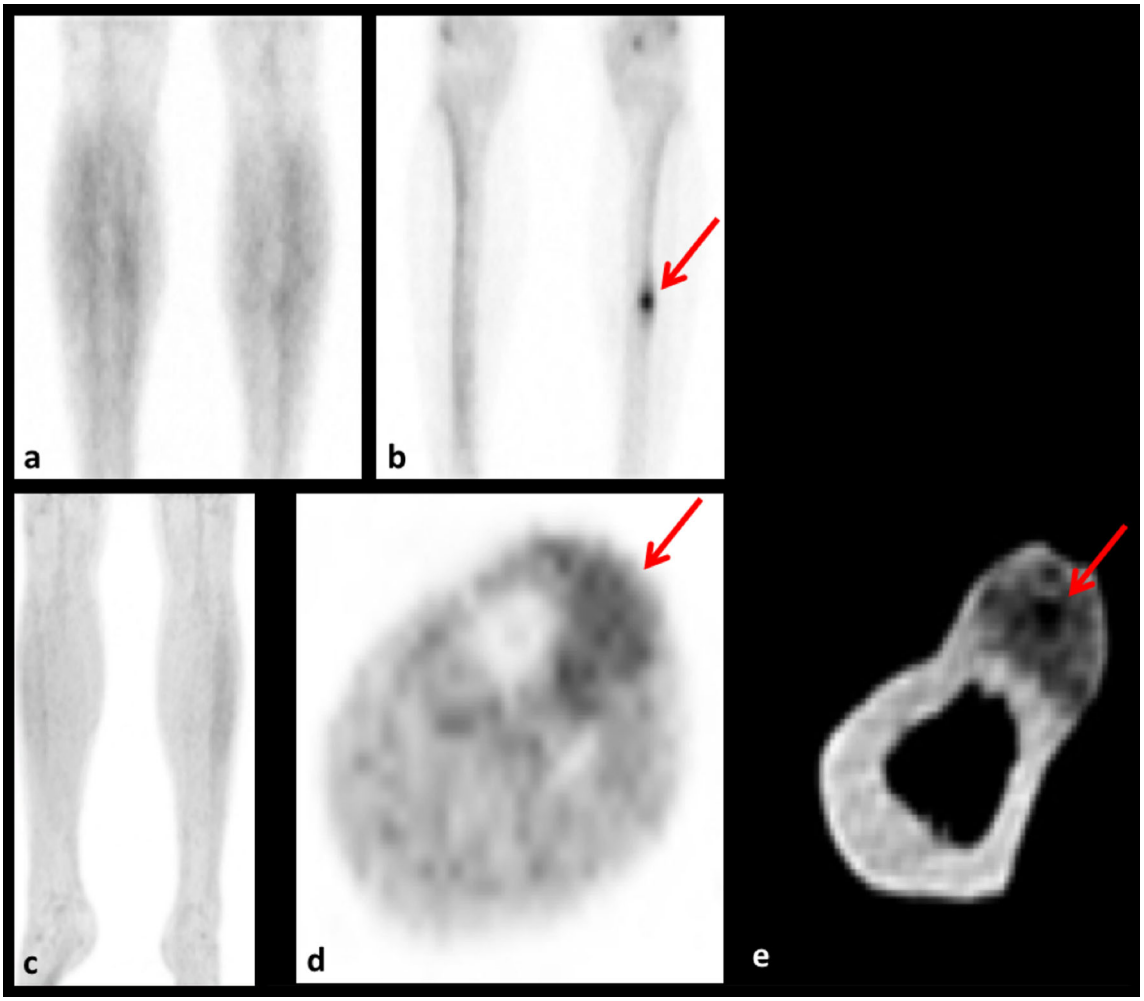

Fig. 13 Osteoid osteoma of the left tibia in a 37-year-old man with pain for 3 months. **a** The early phase planar bone scan image shows no increased uptake. **b** The late phase planar bone scan image shows focal increased uptake (*arrow*). **c**–**e** The FDG PET/CT MIP image (**c**) and the axial PET image (**d**) do not show increased uptake, but the axial CT image (**e**) shows a typical nidus (*arrow*) of a cortical osteoid osteoma. Image courtesy of Dr. Joachim Müller, Nuclear Medicine, Cantonal Hospital St. Gallen, Switzerland

prolonged hospitalization and rehabilitation, and insufficiency fractures at the resection site [10, 24, 72]. More recently, various minimally invasive procedures have been developed. Two common techniques used are image-guided drill excision and RFA [73–76]. RFA has been increasingly used in recent years with success rates greater than 90% [73, 74, 76]. During the RFA procedure, the osteoid osteoma is located with CT guidance and an electrode is advanced into the nidus of the lesion. Thermal heating is then applied at a targeted temperature of 90 °C to destroy the nidus. Other minimally invasive techniques include cryoablation, arthroscopic excision, ethanol injection, laser photocoagulation, microwave ablation and MR-guided focused ultrasound [77, 78].

Conclusion

Osteoid osteomas are benign, often painful bone tumours that are frequently challenging to detect and characterize on plain radiography and even MRI, especially in complex anatomical regions such as the spine, pelvis, wrist and foot. Hybrid imaging (SPECT/CT with ^{99m}Tc-labelled bisphosphonates or PET/CT with ^{18}F-NaF) is highly accurate and provides all

Table 1 Features, advantages and limitations of different imaging modalities

Imaging modality	Features	Advantages	Limitations
Plain radiography	Well-defined small lucent lesions representing the nidus with variable amounts of mineralization, accompanied by cortical thickening and reactive sclerosis	Readily available, low cost, high accuracy in osteoid osteomas in diaphysis of long bones	Detection of osteoid osteomas in the axial skeleton, complex anatomy and near joints limited because of superposition of other structures
CT	Well-defined round or oval nidus with low density, variable amounts of reactive sclerosis and periosteal reaction and new bone formation, prominent cortical vascular channels near nidus ("vascular groove" sign)	Good availability, fast, superior to plain radiography in complex areas such as the spine, pelvis and foot, suitable for treatment planning	Small nidus might be difficult to detect
MRI	Nidus with low signal intensity on T1-weighted images and variable intensity on T2-weighted images, oedema in the adjacent bone marrow, and soft tissue. Joint effusion in juxta-articular lesions. Contrast enhancement of the nidus, adjacent bone marrow, soft tissues, and synovia might be seen	Good availability, no radiation, visualization of soft-tissue reactions (arthritis, oedema)	Nidus might be difficult to detect. Extensive oedema might be misleading, CT more suitable for therapy planning
Planar scintigraphy	"Double density" sign with focal hot spot showing the nidus and surrounding less intense uptake in the reactive bone sclerosis	High sensitivity, good availability	Limited specificity, lack of morphological information, not sufficient for therapy planning
Bone SPECT/CT	Signs of planar scintigraphy and CT combined	Combines high sensitivity of planar scintigraphy and specificity of CT to give high accuracy	Availability, cost
^{18}F-NaF PET/CT	Same signs as in SPECT/CT, "double density" sign might be less pronounced because of higher lesion to background uptake ratio	Combines high sensitivity of PET and specificity of CT to give high accuracy	Availability, cost, reimbursement
^{18}F-FDG PET/CT	Variable amount of FDG uptake from silent to high focal uptake of the nidus	Good availability of the tracer FDG	Most osteoid osteomas not FDG active, not recommended and reimbursed in most countries, cost

Table 2 Differential diagnoses and their features with different imaging modalities

Entity	Plain radiography	CT	MRI	Planar scintigraphy	SPECT/CT	^{18}F-NaF PET/CT	^{18}F-FDG PET/CT
Brodie's abscess/-osteomyelitis	Radiolucent lesion more irregular in shape with indistinct/hazy inner margins, usually intramedullary, but might appear in cortex	Radiolucent lesion more irregular in shape with indistinct/hazy inner margins, usually intramedullary, but might appear in cortex	Low signal on T1, high signal on T2. Peripheral rim contrast enhancement, centre of abscess does not enhance	Increased uptake in early and late phases	Combination of CT and scintigraphy features	High focal uptake combined with CT signs	Increased FDG uptake combined with CT signs
Stress fracture	Linear radiolucent line or sclerosis with periosteal reaction	Linear radiolucent line or sclerosis with periosteal reaction	Low signal fracture line on T1 and T2 with surrounding bone marrow oedema and periosteal reaction, sometimes no fracture line visible	Increased linear uptake	Combination of CT and scintigraphy features	High linear uptake combined with CT signs	Low linear uptake combined with CT signs
Osteoblastoma	Expansile, larger (>2 cm) than osteoid osteoma, more frequent in spine (neural arch), lucent centre with sclerotic rim, variable amount of mineralization	Expansile, larger (>2 cm) than osteoid osteoma, more frequent in spine (neural arch), lucent centre with sclerotic rim, variable amount of mineralization	Low/intermediate signal on T1, low to high on T2, variable contrast enhancement, prominent peritumoral oedema, periosteal reaction common	Increased uptake in early and late phases	Combination of CT and scintigraphy features	High lesion uptake combined with CT signs	Increased FDG uptake combined with CT signs
Adamantinoma	Typically osteolytic, multilobulated, expansile lesion in the anterior cortex of the tibia	Might additionally show cortical breakthrough and soft-tissue mass	Might show daughter lesions in same bone or fibula, marrow involvement, contrast enhancement	Increased uptake in early and late phases	Combination of CT and scintigraphy features	High lesion uptake combined with CT signs	Increased FDG uptake combined with CT signs
Chondroblastoma	Geographic osteolytic lesion in long bones (humerus, tibia, femur), typically eccentric in the epiphysis, sclerotic margin, intramedullary, often periosteal reaction	Often chondroid matrix, no cortical breakthrough	Low signal on T1, inhomogeneous signal on T2, occasionally fluid levels because of secondary aneurysmal bone cyst, periosteal reaction in adjacent metaphysis	Increased uptake in early and late phases	Combination of CT and scintigraphy features	High lesion uptake combined with CT signs	Increased FDG uptake combined with CT signs

the necessary functional information for diagnosis, as well as morphological information to guide treatment.

Acknowledgments Figure 12: Image courtesy of Dr. Alessio Imperiale, Nuclear Medicine, University Hospital Strasbourg, France.

Figure 13: Image courtesy of Dr. Joachim Müller, Nuclear Medicine, Cantonal Hospital St. Gallen, Switzerland.

Figures 7 and 9: Image design courtesy of Lutz Lehmann, Luzerner Kantonsspital, Luzern, Switzerland.

Authors' contributions All authors contributed in a significant way to the content and revision of this manuscript. All authors read and approved the final manuscript.

Compliance with ethical standards

Conflicts of interest None.

Ethical approval and consent to participate Not applicable.

Consent to publication Not applicable.

References

1. Bergstrand H. Uber eine eigenartige, wahrscheinlich bisher nicht beschriebene osteoblastiche krankheit in den langen knochen der hand und des fusses. Acta Radiol. 1930;11:596–613.
2. Jaffe H. Osteoid osteoma: a benign osteoblastic tumor composed of osteoid and atypical bone. Arch Surg. 1935;31:709–28.
3. Klein MH, Shankman S. Osteoid osteoma: radiologic and pathologic correlation. Skelet Radiol. 1992;21:23–31.
4. Loizaga JM, Calvo M, Lopez BF, Martinez TFJ, Perez VJ. Osteoblastoma and osteoid osteoma: clinical and morphological features of 162 cases. Pathol Res Pract. 1993;189:33–41.
5. Steiner GC. Ultrastructure of osteoid osteoma. Hum Pathol. 1976;7:309–25.
6. Kayser F, Resnick D, Haghighi P, Pereira E, Greenway G, Schweitzer M, et al. Evidence of the subperiosteal origin of osteoid osteomas in tubular bones: analysis by CT and MR imaging. AJR Am J Roentgenol. 1998;170:609–14.
7. Chai JW, Hong SH, Choi JY, Koh YH, Lee JW, Choi JA, et al. Radiologic diagnosis of osteoid osteoma: from simple to challenging findings. Radiographics. 2010;30(3):737–49. https://doi.org/10.1148/rg.303095120.
8. Iyer RS, Chapman T, Chew FS. Pediatric bone imaging: diagnostic imaging of osteoid osteoma. AJR Am J Roentgenol. 2012;198(5):1039–52. https://doi.org/10.2214/AJR.10.7313.
9. Kransdorf MJ, Stull MA, Gilkey FW, Moser RP Jr. Osteoid osteoma. Radiographics. 1991;11(4):671–96. https://doi.org/10.1148/radiographics.11.4.1887121.
10. Kneisl JS, Simon MA. Medical management compared with operative treatment for osteoid-osteoma. J Bone Joint Surg Am. 1992;74:179–85.
11. Laurence N, Epelman M, Markowitz RI, Jaimes C, Jaramillo D, Chauvin NA. Osteoid osteomas: a pain in the night diagnosis. Pediatr Radiol. 2012;42(12):1490–501. https://doi.org/10.1007/s00247-012-2495-y.
12. Lee EH, Shafi M, Hui JH. Osteoid osteoma: a current review. J Pediatr Orthop. 2006;26(5):695–700. https://doi.org/10.1097/01.bpo.0000233807.80046.7c.
13. Swee RG, McLeod RA, Beabout JW. Osteoid osteoma. Detection, diagnosis, and localization. Radiology. 1979;130:117–23.
14. Ebrahim FS, Jacobson JA, Lin J, Housner JA, Hayes CW, Resnick D. Intraarticular osteoid osteoma: sonographic findings in three patients with radiographic, CT, and MR imaging correlation. AJR Am J Roentgenol. 2001;177:1391–5.
15. Gil S, Marco SF, Arenas J, Irurzun J, Agullo T, Alonso S, et al. Doppler duplex color localization of osteoid osteomas. Skelet Radiol. 1999;28:107–10.
16. Helms CA, Hattner RS, Vogler JB. Osteoid osteoma: radionuclide diagnosis. Radiology. 1984;151:779–84.
17. Lindbom A, Lindvall N, Soderberg G, Spjut H. Angiography in osteoid osteoma. Acta Radiol. 1960;54:327–33.
18. von Kalle T, Langendorfer M, Fernandez FF, Winkler P. Combined dynamic contrast-enhancement and serial 3D-subtraction analysis in magnetic resonance imaging of osteoid osteomas. Eur Radiol. 2009;19(10):2508–17. https://doi.org/10.1007/s00330-009-1430-6.
19. Greco F, Tamburrelli F, Ciabattoni G. Prostaglandins in osteoid osteoma. Int Orthop. 1991;15:35–7.
20. Mungo DV, Zhang X, O'Keefe RJ. COX-1 and COX-2 expression in osteoid osteomas. J Orthop Res. 2002;20:159–62.
21. Gautschi M, Strobel K, Schoniger R, Pfeiffer D, Schmid L. A special case of monoarthritis of the elbow. Z Rheumatol. 2017;76(7):636–9. https://doi.org/10.1007/s00393-017-0359-4.
22. Basu S, Basu P, Dowell J. Painless osteoid osteoma in a metacarpal. J Hand Surg Br. 1999;24:133–4.
23. Ekmekci P, Bostanci S, Erdogan N, Akcaboy B, Guergey E. A painless subungual osteoid osteoma. Dermatol Surg. 2001;27:764–5.
24. Papathanassiou ZG, Megas P, Petsas T, Papachristou DJ, Nilas J, Siablis D. Osteoid osteoma: diagnosis and treatment. Orthopedics. 2008;31(11):1118.
25. Edeiken J, DePalma AF, Hodes PJ. Osteoid osteoma. (Roentgenographic emphasis). Clin Orthop Relat Res. 1966;49:201–6.
26. Graham GN, Browne H. Primary bony tumors of the pediatric spine. Yale J Biol Med. 2001;74(1):1–8.
27. Healey JH, Ghelman B. Osteoid osteoma and osteoblastoma. Current concepts and recent advances. Clin Orthop Relat Res. 1986;204:76–85.
28. Ghanem I. The management of osteoid osteoma: updates and controversies. Curr Opin Pediatr. 2006;18(1):36–41. https://doi.org/10.1097/01.mop.0000193277.47119.15.
29. Gamba JL, Martinez S, Apple J, Harrelson JM, Nunley JA. Computed tomography of axial skeletal osteoid osteomas. AJR Am J Roentgenol. 1984;142(4):769–72. https://doi.org/10.2214/ajr.142.4.769.
30. Harish S, Saifuddin A. Imaging features of spinal osteoid osteoma with emphasis on MRI findings. Eur Radiol. 2005;15(12):2396–403. https://doi.org/10.1007/s00330-005-2816-8.
31. Jordan RW, Koc T, Chapman AW, Taylor HP. Osteoid osteoma of the foot and ankle – a systematic review. Foot Ankle Surg. 2015;21(4):228–34. https://doi.org/10.1016/j.fas.2015.04.005.
32. Athwal GS, Pichora DR, Ellis RE, Rudan JF. A computer-assisted guidance technique for the localization and excision of osteoid osteoma. Orthopedics. 2004;27(2):195–7.
33. Liu PT, Kujak JL, Roberts CC, de Chadarevian JP. The vascular groove sign: a new CT finding associated with osteoid osteomas. AJR Am J Roentgenol. 2011;196(1):168–73. https://doi.org/10.2214/AJR.10.4534.
34. Levine E, Neff JR. Dynamic computed tomography scanning of benign bone lesions: preliminary results. Skelet Radiol. 1983;9(4):238–45.

35. McGrath BE, Bush CH, Nelson TE, Scarborough MT. Evaluation of suspected osteoid osteoma. Clin Orthop Relat Res. 1996;327:247–52.
36. Assoun J, Richardi G, Railhac JJ, Baunin C, Fajadet P, Giron J, et al. Osteoid osteoma: MR imaging versus CT. Radiology. 1994;191(1):217–23. https://doi.org/10.1148/radiology.191.1.8134575.
37. Davies M, Cassar-Pullicino VN, Davies AM, McCall IW, Tyrrell PN. The diagnostic accuracy of MR imaging in osteoid osteoma. Skelet Radiol. 2002;31(10):559–69. https://doi.org/10.1007/s00256-002-0546-4.
38. Zanetti M, Eberhard SM, Exner GU, von Hochstetter A, Hodler J. Magnetic resonance tomography in osteoid osteoma: more confusion than benefit?. Praxis (Bern 1994). 1997;86(11):432–6.
39. Liu PT, Chivers FS, Roberts CC, Schultz CJ, Beauchamp CP. Imaging of osteoid osteoma with dynamic gadolinium-enhanced MR imaging. Radiology. 2003;227(3):691–700. https://doi.org/10.1148/radiol.2273020111.
40. Wells RG, Miller JH, Sty JR. Scintigraphic patterns in osteoid osteoma and spondylolysis. Clin Nucl Med. 1987;12(1):39–44.
41. Park JH, Pahk K, Kim S, Lee SH, Song SH, Choe JG. Radionuclide imaging in the diagnosis of osteoid osteoma. Oncol Lett. 2015;10(2):1131–4. https://doi.org/10.3892/ol.2015.3258.
42. Helms CA. Osteoid osteoma. The double density sign. Clin Orthop Relat Res. 1987;222:167–73.
43. Roach PJ, Connolly LP, Zurakowski D, Treves ST. Osteoid osteoma: comparative utility of high-resolution planar and pinhole magnification scintigraphy. Pediatr Radiol. 1996;26(3):222–5.
44. Banzo I, Montero A, Uriarte I, Vallina NK, Hernandez A, Guede C, et al. Localization by bone SPET of osteoid osteoma in the vertebral lamina. Rev Esp Med Nucl. 1999;18(1):47–9.
45. Ryan PJ, Fogelman I. Bone SPECT in osteoid osteoma of the vertebral lamina. Clin Nucl Med. 1994;19(2):144–5.
46. Hasegawa BH, Wong KH, Iwata K, Barber WC, Hwang AB, Sakdinawat AE, et al. Dual-modality imaging of cancer with SPECT/CT. Technol Cancer Res Treat. 2002;1(6):449–58. https://doi.org/10.1177/153303460200100605.
47. Mariani G, Bruselli L, Kuwert T, Kim EE, Flotats A, Israel O, et al. A review on the clinical uses of SPECT/CT. Eur J Nucl Med Mol Imaging. 2010;37(10):1959–85. https://doi.org/10.1007/s00259-010-1390-8.
48. Farid K, El-Deeb G, Caillat Vigneron N. SPECT-CT improves scintigraphic accuracy of osteoid osteoma diagnosis. Clin Nucl Med. 2010;35(3):170–1. https://doi.org/10.1097/RLU.0b013e3181cc648f.
49. Sharma P, Mukherjee A, Karunanithi S, Nadarajah J, Gamanagatti S, Khan SA, et al. 99mTc-methylene diphosphonate SPECT/CT as the one-stop imaging modality for the diagnosis of osteoid osteoma. Nucl Med Commun. 2014;35(8):876–83. https://doi.org/10.1097/MNM.0000000000000134.
50. Squier SB, Lewis JI, Accurso JM, Jain MK. (99m)Tc-methylene diphosphonate single-photon emission computed tomography/computed tomography improves the diagnostic accuracy of osteoid osteoma. Indian J Nucl Med. 2016;31(4):298–300. https://doi.org/10.4103/0972-3919.187459.
51. Beheshti M, Mottaghy FM, Payche F, Behrendt FFF, Van den Wyngaert T, Fogelman I, et al. (18)F-NaF PET/CT: EANM procedure guidelines for bone imaging. Eur J Nucl Med Mol Imaging. 2015;42(11):1767–77. https://doi.org/10.1007/s00259-015-3138-y.
52. Segall G, Delbeke D, Stabin MG, Even-Sapir E, Fair J, Sajdak R, et al. SNM practice guideline for sodium 18F-fluoride PET/CT bone scans 1.0. J Nucl Med. 2010;51(11):1813–20. https://doi.org/10.2967/jnumed.110.082263.
53. Even-Sapir E, Metser U, Mishani E, Lievshitz G, Lerman H, Leibovitch I. The detection of bone metastases in patients with high-risk prostate cancer: 99mTc-MDP planar bone scintigraphy, single- and multi-field-of-view SPECT, 18F-fluoride PET, and 18F-fluoride PET/CT. J Nucl Med. 2006;47(2):287–97.
54. Shen CT, Qiu ZL, Han TT, Luo QY. Performance of 18F-fluoride PET or PET/CT for the detection of bone metastases: a meta-analysis. Clin Nucl Med. 2015;40(2):103–10. https://doi.org/10.1097/RLU.0000000000000592.
55. Strobel K, Fischer DR, Tamborrini G, Kyburz D, Stumpe KD, Hesselmann RG, et al. 18F-fluoride PET/CT for detection of sacroiliitis in ankylosing spondylitis. Eur J Nucl Med Mol Imaging. 2010;37(9):1760–5. https://doi.org/10.1007/s00259-010-1464-7.
56. Fischer DR, Maquieira GJ, Espinosa N, Zanetti M, Hesselmann R, Johayem A, et al. Therapeutic impact of [(18)F]fluoride positron-emission tomography/computed tomography on patients with unclear foot pain. Skelet Radiol. 2010;39(10):987–97. https://doi.org/10.1007/s00256-010-0875-7.
57. Drubach LA, Johnston PR, Newton AW, Perez-Rossello JM, Grant FD, Kleinman PK. Skeletal trauma in child abuse: detection with 18F-NaF PET. Radiology. 2010;255(1):173–81. https://doi.org/10.1148/radiol.09091368.
58. Dasa V, Adbel-Nabi H, Anders MJ, Mihalko WM. F-18 fluoride positron emission tomography of the hip for osteonecrosis. Clin Orthop Relat Res. 2008;466(5):1081–6. https://doi.org/10.1007/s11999-008-0219-2.
59. Dua SG, Purandare NC, Shah S, Rangarajan V. F-18 fluoride PET/CT in the detection of radiation-induced pelvic insufficiency fractures. Clin Nucl Med. 2011;36(10):e146–9. https://doi.org/10.1097/RLU.0b013e31821a293b.
60. Brenner W, Vernon C, Conrad EU, Eary JF. Assessment of the metabolic activity of bone grafts with (18)F-fluoride PET. Eur J Nucl Med Mol Imaging. 2004;31(9):1291–8. https://doi.org/10.1007/s00259-004-1568-z.
61. Grant FD. (18)F-fluoride PET and PET/CT in children and young adults. PET Clin. 2014;9(3):287–97. https://doi.org/10.1016/j.cpet.2014.03.004.
62. Strobel K, Vali R. (18)F NaF PET/CT versus conventional bone scanning in the assessment of benign bone disease. PET Clin. 2012;7(3):249–61. https://doi.org/10.1016/j.cpet.2012.04.007.
63. Even-Sapir E, Mishani E, Flusser G, Metser U. 18F-fluoride positron emission tomography and positron emission tomography/computed tomography. Semin Nucl Med. 2007;37(6):462–9. https://doi.org/10.1053/j.semnuclmed.2007.07.002.
64. Lim CH, Park YH, Lee SY, Chung SK. F-18 FDG uptake in the nidus of an osteoid osteoma. Clin Nucl Med. 2007;32(8):628–30. https://doi.org/10.1097/RLU.0b013e3180a1acf3.
65. Imperiale A, Moser T, Ben-Sellem D, Mertz L, Gangi A, Constantinesco A. Osteoblastoma and osteoid osteoma: morphofunctional characterization by MRI and dynamic F-18 FDG PET/CT before and after radiofrequency ablation. Clin Nucl Med. 2009;34(3):184–8. https://doi.org/10.1097/RLU.0b013e3181966de6.
66. Aoki J, Watanabe H, Shinozaki T, Takagishi K, Ishijima H, Oya N, et al. FDG PET of primary benign and malignant bone tumors: standardized uptake value in 52 lesions. Radiology. 2001;219(3):774–7. https://doi.org/10.1148/radiology.219.3.r01ma08774.
67. Strobel K, Hany TF, Exner GU. PET/CT of a Brodie abscess. Clin Nucl Med. 2006;31(4):210. https://doi.org/10.1097/01.rlu.0000204125.79919.44.
68. Hudson TM, Hawkins IF Jr. Radiological evaluation of chondroblastoma. Radiology. 1981;139(1):1–10. https://doi.org/10.1148/radiology.139.1.7208908.
69. Atesok KI, Alman BA, Schemitsch EH, Peyser A, Mankin H. Osteoid osteoma and osteoblastoma. J Am Acad Orthop Surg. 2011;19(11):678–89.
70. Moberg E. The natural course of osteoid osteoma. J Bone Joint Surg Am. 1951;33 A(1):166–70.

71. Goto T, Shinoda Y, Okuma T, Ogura K, Tsuda Y, Yamakawa K, et al. Administration of nonsteroidal anti-inflammatory drugs accelerates spontaneous healing of osteoid osteoma. Arch Orthop Trauma Surg. 2011;131(5):619–25. https://doi.org/10.1007/s00402-010-1179-z.
72. Rosenthal DI, Hornicek FJ, Torriani M, Gebhardt MC, Mankin HJ. Osteoid osteoma: percutaneous treatment with radiofrequency energy. Radiology. 2003;229(1):171–5. https://doi.org/10.1148/radiol.2291021053.
73. Lindner NJ, Ozaki T, Roedl R, Gosheger G, Winkelmann W, Wortler K. Percutaneous radiofrequency ablation in osteoid osteoma. J Bone Joint Surg Br. 2001;83(3):391–6.
74. Rosenthal DI, Springfield DS, Gebhardt MC, Rosenberg AE, Mankin HJ. Osteoid osteoma: percutaneous radio-frequency ablation. Radiology. 1995;197(2):451–4. https://doi.org/10.1148/radiology.197.2.7480692.
75. Sans N, Galy-Fourcade D, Assoun J, Jarlaud T, Chiavassa H, Bonnevialle P, et al. Osteoid osteoma: CT-guided percutaneous resection and follow-up in 38 patients. Radiology. 1999;212(3):687–92. https://doi.org/10.1148/radiology.212.3.r99se06687.
76. Woertler K, Vestring T, Boettner F, Winkelmann W, Heindel W, Lindner N. Osteoid osteoma: CT-guided percutaneous radiofrequency ablation and follow-up in 47 patients. J Vasc Interv Radiol. 2001;12(6):717–22.
77. Kostrzewa M, Diezler P, Michaely H, Rathmann N, Attenberger UI, Schoenberg SO, et al. Microwave ablation of osteoid osteomas using dynamic MR imaging for early treatment assessment: preliminary experience. J Vasc Interv Radiol. 2014;25(1):106–11. https://doi.org/10.1016/j.jvir.2013.09.009.
78. Napoli A, Bazzocchi A, Scipione R, Anzidei M, Saba L, Ghanouni P, et al. Noninvasive therapy for osteoid osteoma: a prospective developmental study with MR imaging-guided high-intensity focused ultrasound. Radiology. 2017;285(1):186–96. https://doi.org/10.1148/radiol.2017162680.